JOURNAL OF COMPUTATIONAL PHYSICS 23, 300–312 (1977)

A Self-Consistent Magnetostatic Particle Code for Numerical Simulation of Plasmas

J. BUSNARDO-NETO,* P. L. PRITCHETT,†
A. T. LIN, AND J. M. DAWSON

Department of Physics, University of California, Los Angeles, California 90024

Received May 10, 1976; revised July 30, 1976

A particle simulation code has been developed which is particularly well suited for the investigation of low-frequency plasma phenomena. The code is based on Darwin's formulation of Maxwell's equations in which the transverse displacement current is neglected. There is thus no radiation, but the self-consistent magnetic fields are retained. Use is made of the particle equation of motion to transform the Darwin field equations into a set that is stable under integration in time. An iteration procedure is developed for solving these equations at each time step. This scheme has been coded using finite-size particles and fast Fourier transform methods in both $1\frac{2}{2}$ and $2\frac{1}{2}$ dimensions. The codes have been checked by comparing the simulation results with the dispersion relations for Alfvén, whistler, and magnetosonic waves. Good agreement was obtained.

1. INTRODUCTION

The use of computer simulation models to perform numerical experiments is a powerful tool in plasma physics. Numerical experiments are used together with theoretical analysis and laboratory experiments in the study of basic plasma phenomena. One type of model consists of the so-called particle-pushing simulation codes. In these codes the trajectories of a large number of charged particles are followed in time. The particles move under the influence of their self-consistent fields as well as any external fields. Usually these codes are either purely electrostatic or fully electromagnetic. In the electrostatic codes the only self-consistent fields present are those obtained from Poisson's equation. These codes can be used to investigate those low-frequency phenomena where electrostatic effects are dominant [1–4]. However, they suffer the obvious limitation of neglecting the self-consistent magnetic fields, thereby excluding a whole range of interesting plasma problems. In the electromagnetic codes the full set of Maxwell's equations is solved to obtain the self-consistent fields. Although they are very good for investigating problems involving radiation [5–8], these codes suffer from excessive bremsstrahlung (due to the highly particulate nature

* Present address: Instituto de Fisica, Universidade Estadual de Campinas, 13100 Campinas, SP, Brasil.

† NSF postdoctoral Energy-Related Fellow.

ISSN 0021-9991

of the model). Also the time step has to be small in order to resolve the high frequencies of the electromagnetic waves. Therefore an excessive number of time steps is needed to simulate low-frequency phenomena. The computer runs are then too long (and too expensive), and there is an unacceptable accumulation of errors.

A model which incorporates the self-consistent magnetic fields and is appropriate for low frequencies is the Darwin model [9, 10]. In this model the transverse part of the displacement current is neglected in Ampère's law. This is the only approximation made; the remaining Maxwell's equations are used in their exact form. The Darwin formulation is correct to order $(v/c)^2$ and includes electrostatic and magnetostatic effects and electromagnetic induction, but neglects radiation. It is sometimes called a nonradiative or self-inductive model. Earlier applications of this formulation to particle-pushing codes were restricted to one-dimensional cases [11] and made use of the conservation of the transverse canonical momentum [12, 13]. Haber *et al.* [14] extended the approach to one-dimensional situations in which the canonical momentum was not strictly conserved. This code was used to study whistlers [15] and also instabilities in unmagnetized, anisotropic plasmas [16]. More recently, Denavit [17] developed a sophisticated code, still in one dimension, using the Darwin Lagrangian and incorporating quiet starts and charge-weighted particles.

In the one-dimensional codes there is only one direction for wave propagation, and it is simple to separate all vector quantities into parallel and transverse components. It is also possible to displace the particle and field quantities in time so as to obtain perfect time centering. However, the methods used in [11–14, 17] do not generalize to more than one dimension, since the canonical momentum is conserved only in the direction of ignorable spatial coordinates and in general there are an insufficient number of such coordinates. In this paper we present an alternate approach which appears to be similar to that developed by Nielson and Lewis [18]. The scheme has been coded in both one-and-two-halves dimensions (one position, three velocities) and in two-and-one-half dimensions (two positions, three velocities). The model uses Gaussian-shaped particles to represent the plasma. This results in the suppression of short-wavelength fluctuations. A fast Fourier transform algorithm is used to solve for the fields, thus allowing a very natural separation into components parallel and perpendicular to the direction of propagation. A straightforward integration in time of Darwin's formulation of the electromagnetic equations leads to a numerical instability [14, 18], which in the one-dimensional models can be suppressed in different ways [12–14, 17]. The instability is caused by the fact that the inductive fields which arise from the acceleration of particles strongly modify the acceleration. Here we present a scheme in which the time derivative in the field equations is eliminated by means of the equation of motion of the particles. The resulting equation for the transverse electric field is fairly complicated, but we have derived a successful iterative procedure for solving it. The iteration is in space, not time, and convergence is very rapid for uniform density plasmas. Even for strongly nonuniform plasmas the convergence is satisfactory. The one-dimensional code was used to study the absorption of ion cyclotron waves [19] and is also applicable to loss-cone studies in mirror machines and multimirror confinement schemes. The two-dimensional version is being used current-

ly to study Alfvén waves in nonuniform plasmas. The results will appear elsewhere. The present paper concentrates on the mathematical formulation and numerical aspects of the magnetostatic scheme.

2. The Model

It is well known that a vector quantity can be separated into two components; one is divergence free (transverse), the other is curl free (longitudinal). We separate the electromagnetic fields and the current density in this way and denote the resulting components by the subscripts T and L. Then the equations for the electromagnetic fields in Darwin's approximation are written as

$$\nabla \cdot \mathbf{E}_L = 4\pi\rho, \tag{1a}$$

$$c\nabla \times \mathbf{B}_T = 4\pi\mathbf{J}_T, \tag{1b}$$

$$c\nabla \times \mathbf{E}_T = -\partial\mathbf{B}_T/\partial t. \tag{1c}$$

Note in particular the absence of the term $\partial\mathbf{E}_T/\partial t$ in (1b). This is the basic approximation in this radiation-free formulation. The electromagnetic energy and momentum in this approximation are $(8\pi)^{-1}\int (E_L^2 + B_T^2)\,d\mathbf{r}$ and $(4\pi c)^{-1}\int (\mathbf{E}_L \times \mathbf{B}_T)\,d\mathbf{r}$, respectively. The system of Eqs. (1) is supplemented by

$$\nabla \times \mathbf{E}_L = 0, \tag{2a}$$

$$\nabla \cdot \mathbf{B}_T = 0, \tag{2b}$$

$$4\pi\mathbf{J}_L + \partial\mathbf{E}_L/\partial t = 0. \tag{2c}$$

Equations (2a) and (2b) follow from the definitions of longitudinal and transverse components. Equation (2c) is the longitudinal counterpart to (1b) and is a restatement of conservation of charge, a constraint that clearly has to be satisfied.

The longitudinal electric field $\mathbf{E}_L$ is obtained from Eqs. (1a) and (2a); the transverse magnetic field $\mathbf{B}_T$ is obtained from (1b) and (2b). There are no complications involved in these operations. The difficulty lies in the evaluation of the transverse electric field $\mathbf{E}_T$ by means of (1c). A straightforward integration in time leads to a numerical instability. This instability is a well-known problem of the Darwin model. We discuss one possible method of obtaining $\mathbf{E}_T$ in Section 3.

The sources for $\mathbf{E}_L$ and $\mathbf{B}_T$ are the charge density ρ and the transverse current density $\mathbf{J}_T$, respectively. The model described here uses finite-size Gaussian-shaped particles to represent the plasma. It has been shown that finite-size particles are very effective in reducing the anomalously high collision frequencies and suppressing the small-wavelength fluctuations which are inherent to particle codes [20, 21]. The charge density is given by

$$\rho(\mathbf{r}) = \sum_i q_i f(\mathbf{r} - \mathbf{r}_i), \tag{3}$$

and the total current density by

$$\mathbf{J}(\mathbf{r}) = \sum_i q_i \mathbf{v}_i f(\mathbf{r} - \mathbf{r}_i). \tag{4}$$

The summations are performed over all particles. q_i and $\mathbf{v}_i$ are the charge and velocity of the ith particle, while $f(\mathbf{r} - \mathbf{r}_i)$ represents the spatial distribution of charge about the central point $\mathbf{r}_i$ of the particle. For the $2\frac{1}{2}$-dimensional model $\mathbf{r}$ represents a pair of coordinates (x, y), while $\mathbf{v}$ represents the three components of the velocity (v_x, v_y, v_z). The explicit form we use for f is a Gaussian of radius a,

$$f(\mathbf{r} - \mathbf{r}_i) = (2\pi a^2)^{-1} \exp[-(x - x_i)^2/2a^2 - (y - y_i)^2/2a^2]. \tag{5}$$

However, any other convenient form for f could be used.

In order to make the field calculations efficient, a spatial grid is introduced and particle positions $\mathbf{r}_i$ are expressed in terms of the nearest grid point $\mathbf{r}_g$ and the displacement from that grid point $\Delta\mathbf{r}_i$:

$$\mathbf{r}_i = \mathbf{r}_g + \Delta\mathbf{r}_i .$$

The sums indicated in (3) and (4) are then performed following a modified dipole expansion technique known as the subtracted dipole scheme (SUDS) [22]. In this scheme the charge and current densities are accumulated at each grid point using the dipole approximation, and the derivatives of the form factor are approximated by a centered difference over adjacent cells. The charge density thus has the form

$$\rho(\mathbf{r}) = \sum_g f(\mathbf{r} - \mathbf{r}_g)\{\rho_{\mathrm{NGP}}(g) + (1/2\delta)[\rho_{\mathrm{D}}{}^x(m - 1, n) - \rho_{\mathrm{D}}{}^x(m + 1, n) + \rho_{\mathrm{D}}{}^y(m, n - 1) - \rho_{\mathrm{D}}{}^y(m, n + 1)]\}. \tag{6}$$

The summation is over all points $g = (m, n)$ in the two-dimensional grid, and δ is the grid spacing. The monopole part of the expansion is

$$\rho_{\mathrm{NGP}}(g) = \sum_{i \in g} q_i \tag{7}$$

and the dipole terms are given by

$$\begin{aligned} \rho_{\mathrm{D}}{}^x(m, n) &= \sum_{i \in g} q_i \Delta x_i , \\ \rho_{\mathrm{D}}{}^y(m, n) &= \sum_{i \in g} q_i \Delta y_i , \end{aligned} \tag{8}$$

where $i \epsilon g$ indicates that particle i is centered in the gth cell. The current density $\mathbf{J}$ is described by equations of the same form as (6) to (8). Note that these equations are extensions to $2\frac{1}{2}$ dimensions of the corresponding expressions in [22, 23]. The Fourier transforms $\tilde{\rho}(\mathbf{k})$ and $\tilde{\mathbf{J}}(\mathbf{k})$ can now be obtained by performing single two-dimensional transforms. Thus,

$$\tilde{\rho}(\mathbf{k}) = \exp(-k^2a^2/2)(L_xL_y)^{-1} \sum_g \exp(-i\mathbf{k} \cdot \mathbf{r}_g)[\rho_{\mathrm{NGP}}(g) + \rho_{\mathrm{D}}(g)], \tag{9}$$

where $\rho_D(g)$ is the complete dipole contribution in Eq. (6), and L_x and L_y are the dimensions of the (x, y) grid. The term $\exp(-k^2a^2/2)$ is just the form factor of the finite-size Gaussian particle. The source for the magnetic field is the transverse part of the current density, and this is easily obtained in Fourier space via the operation

$$\tilde{\mathbf{J}}_T(\mathbf{k}) = \tilde{\mathbf{J}}(\mathbf{k}) - \mathbf{k}(\mathbf{k} \cdot \tilde{\mathbf{J}})/k^2. \tag{10}$$

The Fourier components $\tilde{\mathbf{E}}_L(\mathbf{k})$ and $\tilde{\mathbf{B}}_T(\mathbf{k})$ are computed from the sources using the equations

$$i\mathbf{k} \cdot \tilde{\mathbf{E}}_L(\mathbf{k}) = 4\pi\tilde{\rho}(\mathbf{k}), \tag{11a}$$

$$i\mathbf{k} \times \tilde{\mathbf{E}}_L(\mathbf{k}) = 0, \tag{11b}$$

$$ic\mathbf{k} \times \tilde{\mathbf{B}}_T(\mathbf{k}) = 4\pi\tilde{\mathbf{J}}_T(\mathbf{k}), \tag{11c}$$

$$i\mathbf{k} \cdot \tilde{\mathbf{B}}_T(\mathbf{k}) = 0. \tag{11d}$$

The longitudinal electric field and the transverse magnetic field in real space are obtained by means of an inverse Fourier transform. These fields plus the transverse component of **E** (to be discussed in Section 3) and any externally applied fields are used to compute the force on a particle,

$$\begin{aligned}\mathbf{F}(\mathbf{r}_i) &= q_i \int f(\mathbf{r}' - \mathbf{r}_i)[\mathbf{E}(\mathbf{r}') + \mathbf{v}_i \times \mathbf{B}(\mathbf{r}')/c]\, d\mathbf{r}' \\ &= q_i \int \exp(-k^2a^2/2)[\tilde{\mathbf{E}}(\mathbf{k}) + \mathbf{v}_i \times \tilde{\mathbf{B}}(\mathbf{k})/c] \exp(i\mathbf{k} \cdot \mathbf{r}_i)\, d\mathbf{k}.\end{aligned} \tag{12}$$

In the simulation model the fields, and hence the right side of (12), are calculated only at the grid points. To increase the accuracy of the force calculation, a dipole expansion of $\mathbf{r}_i$ around the nearest $\mathbf{r}_g$ is used, in which derivatives of the fields are again approximated by central differences.

After the force $\mathbf{F}(\mathbf{r}_i)$ is obtained, the particle positions and velocities are advanced in time by means of the equations of motion

$$d\mathbf{v}_i/dt = \mathbf{F}(\mathbf{r}_i)/m_i\,, \tag{13a}$$

$$d\mathbf{r}_i/dt = \mathbf{v}_i\,, \tag{13b}$$

using the leapfrog method. Equation (13b) is fully time centered with the velocities defined at the full time steps and the positions defined at the half time steps. We would like to have (13a) also be time centered. The longitudinal part of the electric field is centered since it depends only on the positions. But the transverse fields involve both the positions and velocities (see Eq. (11c) and Section 3); we compute them at the same instant as the velocities. To achieve the desired time centering, we use a first-order Taylor expansion to advance $\mathbf{B}_T(t)$ and $\mathbf{E}_T(t)$ half a time step ahead. This requires that values of the fields be saved from the previous time step. The arrangement ofthe variables in time is shown in Fig. 1. At the beginning of a loop, $\mathbf{r}_{i,n-1/2}$, $\mathbf{v}_{i,n}$, $\mathbf{E}_T^{\text{old}}$, and $\mathbf{B}_T^{\text{old}}$ are known. The procedure is then the following. (i) $\mathbf{r}_i$ is advanced by $\Delta t/2$

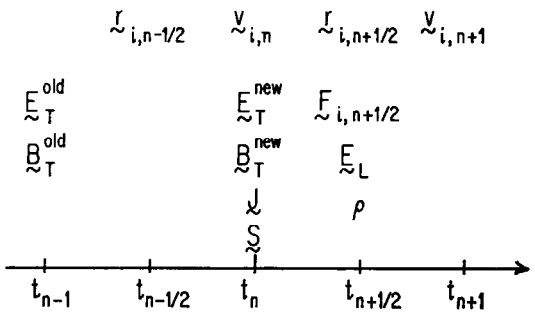

FIG. 1. A diagram illustrating the time advancement of field and particle quantities in the magnetostatic code.

using $\mathbf{v}_{i,n}$, and $\mathbf{J}$ and $\mathbf{S}$ (to be defined in Section 3) are accumulated on the grid points. (ii) $\mathbf{r}_i$ is advanced by the remaining $\Delta t/2$, and ρ is accumulated on the grid points. (iii) The fields $\mathbf{E}_T^{new}$, $\mathbf{B}_T^{new}$, and $\mathbf{E}_L$ are computed in Fourier space and then transformed back to real space. The transverse fields are advanced to $t_{n+1/2}$ using the Taylor expansion. (iv) The force $\mathbf{F}_{i,n+1/2}$ is computed and the velocities are advanced by Δt. We are now back at the beginning, ready to start the next loop.

3. THE COMPUTATION OF E_T

As already mentioned, the straightforward integration in time of Eq. (1) is numerically unstable. In order to eliminate this instability, we have to eliminate the time derivative from Eq. (1c). This is done as follows. First take the curl of (1c) to obtain

$$\nabla^2 \mathbf{E}_T = (4\pi/c^2)(\partial \mathbf{J}/\partial t)_T . \tag{14}$$

Using the definition of $\mathbf{J}$ in Eq. (4), we have

$$\partial \mathbf{J}/\partial t = \sum_i q_i[(\partial \mathbf{v}_i/\partial t) f(\mathbf{r} - \mathbf{r}_i) - \mathbf{v}_i(\mathbf{v}_i \cdot \nabla) f(\mathbf{r} - \mathbf{r}_i)]. \tag{15}$$

We then use the equation of motion to rewrite (15) as

$$\partial \mathbf{J}/\partial t = \sum_i q_i \left[(q_i/m_i) f(\mathbf{r} - \mathbf{r}_i) \int f(\mathbf{r}' - \mathbf{r}_i)\{\mathbf{E}(\mathbf{r}') + \mathbf{v}_i \times \mathbf{B}(\mathbf{r}')/c\}\, d\mathbf{r}' - \mathbf{v}_i(\mathbf{v}_i \cdot \nabla) f(\mathbf{r} - \mathbf{r}_i)\right]. \tag{16}$$

We now take the transverse part of (16) and substitute into (14) to obtain

$$\nabla^2 \mathbf{E}_T - (4\pi/c^2)\left[\sum_i (q_i^2/m_i) f(\mathbf{r} - \mathbf{r}_i) \int f(\mathbf{r}' - \mathbf{r}_i)\, \mathbf{E}(\mathbf{r}')\, d\mathbf{r}'\right]_T = (4\pi/c^2)\left[\sum_i \left\{(q_i^2/m_i) f(\mathbf{r} - \mathbf{r}_i) \int f(\mathbf{r}' - \mathbf{r}_i) \cdot [\mathbf{v}_i \times \mathbf{B}(\mathbf{r}')/c]\, d\mathbf{r}' - q_i \mathbf{v}_i(\mathbf{v}_i \cdot \nabla) f(\mathbf{r} - \mathbf{r}_i)\right\}\right]_T . \tag{17}$$

The right-hand side consists of known quantities and is therefore a source term which we call $-\mathbf{S}_T(\mathbf{r})$. The first term represents a particle flux crossed with the magnetic field, while the second one is the divergence of the current transfer tensor. Neither of these terms normally appears in particle codes, but their computation is straightforward, if tedious. The source term $\mathbf{S}_T(\mathbf{r})$ is accumulated on the grid points from the velocities of the particles. The same SUDS techniques which were used to obtain $\rho(\mathbf{r})$ and $\mathbf{J}(\mathbf{r})$ are used to obtain $\mathbf{S}_T(\mathbf{r})$. The second term on the left-hand side of (17) represents a convolution of the electric field with the number density. Equation (17) is similar to the equation for $\mathbf{E}_T$ obtained by Nielson and Lewis [18]. These authors, however, solve the equation in real space. Reference [14] contains a discussion of this general type of equation.

Since we wish to solve for $\mathbf{E}_T$ in Fourier space, we take the transform of (17). The result is

$$k^2\tilde{\mathbf{E}}_T(\mathbf{k}) + (\omega_{pe}^2/n_0c^2)\exp(-k^2a^2/2)\left\{\sum_{\varkappa}[\tilde{n}_e(\varkappa) + (m_e/m_i)\,\tilde{n}_i(\varkappa)]\right.$$
$$\left.\cdot\,\tilde{\mathbf{E}}(\mathbf{k}-\varkappa)\exp[-(\mathbf{k}-\varkappa)^2a^2/2]\right\}_T$$
$$= \tilde{\mathbf{S}}_T(\mathbf{k}). \tag{18}$$

Here $\tilde{n}_e(\mathbf{k})$ and $\tilde{n}_i(\mathbf{k})$ are the transformed electron and ion number densities, while n_0 is the average electron density. Equation (18) completes the system of equations needed for the magnetostatic model. It can be written in matrix form as

$$[L][E_T] = [S],$$

and so it has a formal solution

$$[E_T] = [L]^{-1}[S].$$

However, it would be prohibitive to invert [L] at every time step for the dimensions usually used in simulation codes. Another possibility is to cut off the higher $\mathbf{k}$ modes, thereby reducing the size of the matrix. However, an inspection of (18) shows that the off-diagonal elements of $[L]$ are of order $\tilde{n}(\mathbf{k})/n_0$ relative to the diagonal terms. Therefore, when the density perturbation is small (i.e., a rather uniform plasma), it is possible to use an iterative procedure. Rewrite (18) keeping the $\kappa = 0$ terms on the left-hand side and transpose the others to the right side. We obtain

$$[k^2 + (\omega_{pe}^2/c^2)(1 + m_e/m_i)\exp(-k^2a^2/2)]\,\tilde{\mathbf{E}}_T(\mathbf{k})$$
$$= \tilde{\mathbf{S}}_T(\mathbf{k}) - (\omega_{pe}^2/n_0c^2)\exp(-k^2a^2/2)\left\{\sum_{\varkappa\neq 0}[\tilde{n}_e(\varkappa) + (m_e/m_i)\,\tilde{n}_i(\varkappa)]\right.$$
$$\left.\cdot\,\tilde{\mathbf{E}}(\mathbf{k}-\varkappa)\exp[-(\mathbf{k}-\varkappa)^2a^2/2]\right\}_T. \tag{19}$$

To begin the iterative procedure, we neglect all the terms on the right side of (19) except $\tilde{\mathbf{S}}_T$. This yields an initial estimate for $\tilde{\mathbf{E}}_T$,

$$\tilde{\mathbf{E}}_T^0(\mathbf{k}) = [k^2 + (\omega_{pe}^2/c^2)(1 + m_e/m_i)\exp(-k^2a^2/2)]^{-1}\,\tilde{\mathbf{S}}_T(\mathbf{k}).$$

We then substitute this result for $\tilde{\mathbf{E}}_T^0$ back into the right side of (19) and solve to obtain a new estimate of $\tilde{\mathbf{E}}_T$. This iteration can be repeated until the new $\tilde{\mathbf{E}}_T(\mathbf{k})$ differs from the old one by some small amount. For thermal plasmas only two or three iterations were needed to reduce the error to less than 0.1 %.

This iterative procedure for computing $\mathbf{E}_T$ turns out, however, not to be restricted to uniform or nearly uniform plasmas. For a plasma with a sinusoidal density perturbation as large as 60 % (thus producing a factor of four variation between the maximum and minimum density), the number of iterations required for 0.1 % convergence increased to only four or five. The present procedure does break down when the maximum density exceeds twice the average density. A modification of the iterative method which permits such cases to be treated is discussed in Section 5.

4. Tests of the Code

The magnetostatic model described above contains a great wealth of plasma phenomena. In order to test the simulation codes based on this model, we have chosen to study in some detail wave propagation in a magnetized, thermal plasma. The theory of such waves is well known [24], and so comparison of the simulation results with theory provides a good check of the whole procedure.

As mentioned previously, the present scheme has been coded in both $1\frac{2}{2}$ and $2\frac{1}{2}$ dimensions. In the two-dimensional code one can observe propagation at all angles θ between the wavevector $\mathbf{k}$ and the uniform external field $\mathbf{B}_0$ in a single run (subject only to the constraints imposed by the discrete grid). In the one-dimensional code only one value of θ can be observed at a time, but naturally the execution time and storage requirements are much smaller for the 1-D code. The simplest case to consider is $\theta = 0$, namely propagation parallel to the external field. The dispersion relations (in magnetostatic approximation) for transverse waves in a cold plasma are then [12]

$$c^2k_\parallel^2 = -\frac{\omega\omega_{pe}^2}{\omega \mp \omega_{ce}} - \frac{\omega\omega_{pi}^2}{\omega \pm \omega_{ci}}. \tag{20}$$

The upper sign yields the electron cyclotron or whistler waves, while the lower sign gives the ion cyclotron waves. The former waves are right circularly polarized, while the latter are left circularly polarized. In the limit $\omega \ll \omega_{ci}$, the two branches come together to form the linearly polarized Alfvén waves.

Runs were made with both codes to check the dispersion relation (20) and the polarization properties of the waves. Since the results were quite similar, we shall mainly discuss the two-dimensional case and only briefly mention the one-dimensional results. A grid of 32×128 cells was used with the external field oriented parallel to the longer dimension. A total of 4096 each electrons and ions were distributed uniformly in space across this grid with random initial velocities. (In the 1-D case 5120 each electrons and ions were similarly distributed across a system 512 cells long.) The remaining parameters used in the simulation were: ion to electron mass ratio

$m_i/m_e = 4$, $T_i = T_e$, $\lambda_D/\delta = 1$, $c/v_{th}^e \equiv c(kT_e/m_e)^{-1/2} = 5$, $\omega_{ce}/\omega_{pe} = 1.2$, and particle size $a/\delta = 1$. In a run of 1000 time steps ($t = 200\omega_{pe}^{-1}$) the energy conservation was better than 1 %. (Because of the larger number of particles per cell, energy conservation in the 1-D run was an order of magnitude better.) Both cyclotron modes were observed, and they possessed the correct polarization properties. In Fig. 2 the

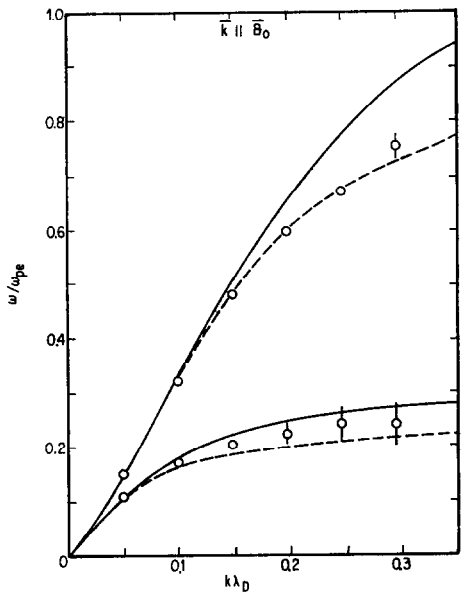

FIG. 2. Dispersion relation for electron and ion cyclotron waves, theory and simulation. Solid lines are for $T = 0$ (Eq. (20)); dashed lines are for finite T (Eq. (21)).

simulation results are compared with the predictions of Eq. (20) modified to include the effect of finite particle size [21] (solid lines). For small values of $k\lambda_D$ there is excellent agreement for both electron and ion cyclotron branches. At larger values of $k\lambda_D$ the electron cyclotron frequencies fall systematically below the cold plasma prediction. This discrepancy is due to thermal effects, as can be seen by solving the finite-temperature dispersion relation [25]

$$c^2k_\parallel^2 = \frac{\omega\omega_{pe}^2}{2^{1/2}kv_{th}^e} Z\left(\frac{\omega \mp \omega_{ce}}{2^{1/2}kv_{th}^e}\right) + \frac{\omega\omega_{pi}^2}{2^{1/2}kv_{th}^i} Z\left(\frac{\omega \pm \omega_{ci}}{2^{1/2}kv_{th}^i}\right). \tag{21}$$

Here Z is the complex plasma dispersion function [26]. The solutions for Re ω are shown in Fig. 2 as dashed lines. There is now excellent agreement for all the electron cyclotron frequencies. For $k\lambda_D \gtrsim 0.2$ the ion cyclotron waves are strongly damped, and it is difficult to determine frequencies from the simulation results.

Next we consider propagation perpendicular to the external field. In the magneto-

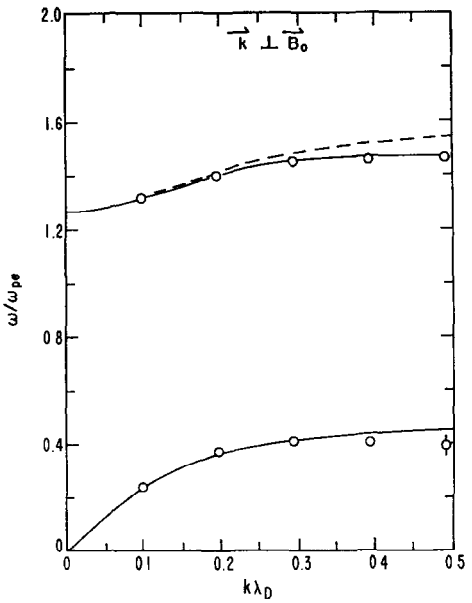

FIG. 3. Dispersion relation for upper and lower hybrid waves, theory and simulation. Solid lines include correction for finite particle size; dashed line does not.

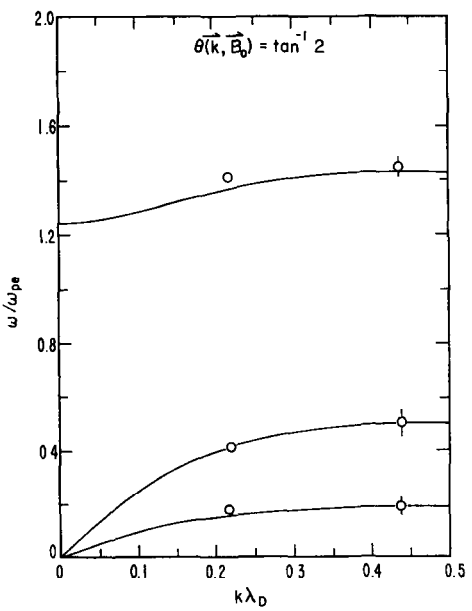

FIG. 4. Dispersion relation for waves propagating at an angle $\tan^{-1} 2$ to the external magnetic field, theory and simulation.

static approximation the ordinary wave does not exist [12]. For the extraordinary wave the cold plasma dispersion relation is

$$c^2k_\perp{}^2 = \frac{\omega^2(\omega_{pe}^2 + \omega_{pi}^2)(\omega_{pe}^2 + \omega_{pi}^2 + \omega_{ce}\omega_{ci} - \omega^2)}{(\omega^2 - \omega_{ce}^2)(\omega^2 - \omega_{ci}^2) - (\omega_{pe}^2 + \omega_{pi}^2)(\omega^2 - \omega_{ci}\omega_{ce})}. \tag{22}$$

Solution of Eq. (22) yields two branches. The lower-frequency branch is the magnetosonic or lower hybrid wave, while the higher-frequency branch is the upper hybrid wave. Figure 3 gives the comparison between theory and the simulation results. The solid curves include the effect of finite particle size and match the computational results very well. The dashed curve, which does not include this effect, indicates the size of this correction. The finite size is clearly apparent in the simulation results.

For propagation at oblique angles to the magnetic field the magnetostatic dispersion relation yields three branches. A representative case is shown in Fig. 4. Once again, the simulation agrees very well with theory.

The evident success of the particle codes in simulating such a diversity of plasma waves and the degree to which energy is conserved give us considerable confidence in the present magnetostatic scheme and its implementation.

5. Nonuniform Densities

A variety of interesting plasma phenomena occur when the density is nonuniform. These include, for instance, cases of wave propagation along or against density gradients and pinch configurations. It would thus be useful to relax the restriction of moderate density perturbations from the iteration procedure of Section 3.

One possibility is to compute $[L]^{-1}$. This will give the correct solution but is prohibitively expensive. Another possibility is suggested by Eq. (18) itself. When reduced to symbolic form, the iteration can be written as

$$[k^2 + \bar{\omega}_{pe}^2/c^2]\,\tilde{\mathbf{E}}_T{}^N = \tilde{\mathbf{S}}_T + [(\omega_{pe}^2 - \bar{\omega}_{pe}^2)/c^2]\,\tilde{\mathbf{E}}_T{}^O, \tag{23}$$

where the superscripts stand for new and old. The term $\bar{\omega}_{pe}^2$ corresponds to the $\tilde{n}(\mathbf{k} = 0)$ term, the average density. The difference $\omega_{pe}^2 - \bar{\omega}_{pe}^2$ corresponds to the terms $\tilde{n}(\mathbf{k})$ with $\mathbf{k} \neq 0$, i.e., the actual density minus its average value. From (23) we obtain $\tilde{\mathbf{E}}_T{}^N$ as

$$\tilde{\mathbf{E}}_T{}^N = \frac{\omega_{pe}^2 - \bar{\omega}_{pe}^2}{k^2c^2 + \bar{\omega}_{pe}^2}\,\tilde{\mathbf{E}}_T{}^O + (k^2 + \bar{\omega}_{pe}^2/c^2)^{-1}\,\tilde{\mathbf{S}}_T\,. \tag{24}$$

For small k this scheme is unstable if $|(\omega_{pe}^2 - \bar{\omega}_{pe}^2)/\bar{\omega}_{pe}^2| > 1$, or $\omega_{pe}^2 > 2\bar{\omega}_{pe}^2$. This can occur if the density fluctuations are large enough so that the peak density is greater than twice the average. To make the iteration stable again, the coefficient of $E_T{}^O$ in (24) has to be made smaller than one. This can be done simply by adding to both

sides of (23) the term ω_{pe}^{m2}, corresponding to the maximum value of the density. The new scheme is then

$$[k^2 + \omega_{pe}^{m2}/c^2]\,\tilde{\mathbf{E}}_T{}^N = \tilde{\mathbf{S}}_T + [(\omega_{pe}^{m2} - \bar{\omega}_{pe}^2)/c^2]\,\tilde{\mathbf{E}}_T{}^O + [(\omega_{pe}^2 - \bar{\omega}_{pe}^2)/c^2]\,\tilde{\mathbf{E}}_T{}^O. \quad (25)$$

It is easy to monitor the peak value of the density during a run and change the value of ω_{pe}^{m2} whenever the instability threshold is approached.

This very simple modification was tried successfully with the one-dimensional code in a test run with a pinch. It was also used in an experiment where ion cyclotron waves of large amplitude were launched into the system at both ends. These waves generated peaks in the density which grew in time and travelled toward the center of the system. The modified iteration scheme described here handled this nonuniform density accurately. Further description and results of this experiment are given in [19].

6. Conclusions

We have developed a magnetostatic particle-pushing simulation code which uses Darwin's formulation of the electromagnetic field equations. This formulation is radiation free, but it retains the low-frequency self-consistent magnetic fields. It is thus appropriate for investigating plasma phenomena occurring in the range normally treated by magnetohydrodynamics. It provides insight into the effects of particle motion (finite-Larmor-radius effects) on results obtained with classical MHD. We have used this formulation in codes with $1\frac{2}{2}$ dimensions and with $2\frac{1}{2}$ dimensions. We have studied propagation, dispersion, and polarization of Alfvén, whistler, and magnetosonic waves. These codes are also being used to study Alfvén waves propagating in a nonuniform plasma and to simulate magnetic mirror machines and multimirror machines. We are just beginning to investigate the wealth of problems to which these codes are applicable.

Acknowledgments

This work was supported by EPRI, Contract No. RP270-2, by ERDA, Contract No. E(11-1) Gen. 10 PA26, and by NSF, Contract No. PHY 74-15233. We are all very happy to acknowledge the invaluable numerical support provided by C. C. Lin and discussions with T. Kamimura.

References

1. R. L. Morse and C. W. Nielson, *Phys. Rev. Lett.* **23** (1969), 1087.
2. W. L. Kruer and J. M. Dawson, *Phys. Fluids* **15** (1972), 446.
3. H. Okuda and J. M. Dawson, *Phys. Fluids* **16** (1973), 408.
4. C. Chu, J. M. Dawson, and H. Okuda, *Phys. Fluids* **18** (1975), 1762.
5. R. L. Morse and C. W. Nielson, *Phys. Fluids* **14** (1971), 830.
6. D. W. Forslund, J. M. Kindel, and E. L. Lindman, *Phys. Rev. Lett.* **30** (1973), 739.
7. W. L. Kruer, K. G. Estabrook, and K. H. Sinz, *Nucl. Fusion* **13** (1973), 952.

8. A. T. LIN AND J. M. DAWSON, *Phys. Fluids* **18** (1975), 201.
9. C. G. DARWIN, *Philos. Mag.* **39** (1920), 537. See also J. D. JACKSON, "Classical Electrodynamics," pp. 409–11, Wiley, New York, 1962.
10. A. N. KAUFMAN AND P. S. ROSTLER, *Phys. Fluids* **14** (1971), 446.
11. A. HASEGAWA AND C. K. BIRDSALL, *Phys. Fluids* **7** (1964), 1590.
12. A. HASEGAWA AND H. OKUDA, *Phys. Fluids* **11** (1968), 1995.
13. D. O. DICKMAN, R. L. MORSE, AND C. W. NIELSON, *Phys. Fluids* **12** (1969), 1708.
14. I. HABER, C. E. WAGNER, J. P. BORIS, AND J. M. DAWSON, A self-consistent electromagnetic particle code, *in* "Proceedings of the Fourth Conference on Numerical Simulation of Plasmas," p. 126, U. S. Government Printing Office, Washington, D. C., 1970.
15. S. L. OSSAKOW, E. OTT, AND I. HABER, *Phys. Fluids* **15** (1972), 2314.
16. R. C. DAVIDSON, D. A. HAMMER, I. HABER, AND C. E. WAGNER, *Phys. Fluids* **15** (1972), 317.
17. J. DENAVIT, *J. Computational Phys.* **15** (1974), 449.
18. C. W. NIELSON AND H. R. LEWIS, Nonradiative electromagnetic particle simulation, *in* "Proceedings of the Seventh Conference on Numerical Simulation of Plasmas," p. 159, New York University, June 1975.
19. J. BUSNARDO-NETO, J. M. DAWSON, T. KAMIMURA, AND A. T. LIN, *Phys. Rev. Lett.* **36** (1976), 28.
20. H. OKUDA AND C. K. BIRDSALL, *Phys. Fluids* **13** (1970), 2123.
21. A. B. LANGDON AND C. K. BIRDSALL, *Phys. Fluids* **13** (1970), 2115.
22. W. L. KRUER, J. M. DAWSON, AND B. ROSEN, *J. Computational Phys.* **13** (1973), 114.
23. A. T. LIN, J. M. DAWSON, AND H. OKUDA, *Phys. Fluids* **17** (1974), 1995.
24. T. H. STIX, "The Theory of Plasma Waves," McGraw–Hill, New York, 1962.
25. S. J. GITOMER AND D. W. FORSLUND, *Phys. Fluids* **17** (1974), 1428.
26. B. D. FRIED AND S. D. CONTE, "The Plasma Dispersion Function," Academic Press, New York, 1961.